This paper appears in Mechatronics, 2023.
https://doi.org/10.1016/j.mechatronics.2023.102949

An Adaptive Multi-objective Motion Distribution Framework for Wheeled Mobile Manipulators via Null-space Exploration*

Hongjun Xing[a,b,c,**], Zhaopei Gong[b,**], Liang Ding[b,*], Ali Torabi[c], Jinbao Chen[a,*], Haibo Gao[b] and Mahdi Tavakoli[c]

[a] College of Astronautics, Nanjing University of Aeronautics and Astronautics, Nanjing 210016, China
[b] State Key Laboratory of Robotics and System, Harbin Institute of Technology, Harbin 150001, China
[c] Department of Electrical and Computer Engineering, University of Alberta, Edmonton T6G 1H9, Alberta, Canada

ARTICLE INFO

Keywords:
Wheeled mobile manipulator
Joint constraints
Multi-objective motion distribution
Task priority
Kinematic redundancy

ABSTRACT

Wheeled mobile manipulators (WMMs) are primarily composed of a manipulator and a mobile base, which lead to their agility, maneuverability, and mobility. Despite impressive progress in recent years, there remains some substantial work in improving WMMs' motion precision, owing to the current limitations in unpredictable wheel slippage, high system redundancy, and absence of external perception information. One intuition is to distribute more of a given set of end-effector motion requirements to the manipulator adaptively – to reduce the motion error introduced by wheel locomotion. With the ultimate goal of improving a WMM's motion accuracy without external perception information, here we present a novel adaptive multi-objective motion distribution framework (AMoMDiF) for a redundant WMM, which is drawn inspiration from null-space exploration. The framework adopts a hierarchical structure to explore the WMM's null space iteratively to achieve three tasks, which are end-effector motion achievement (primary objective), adaptive motion distribution (secondary objective), and manipulability enhancement to avoid singularity (tertiary objective). The secondary objective strives to assign more of an end-effector motion to the manipulator when possible. The tertiary goal will enhance the manipulator's capability to stay away from singularities via the WMM's remaining redundancy after the primary and secondary tasks are completed. Experiment results on a physical platform show that, compared with the traditional motion planning method, the proposed AMoMDiF significantly improves the WMM's motion accuracy through the achievements of the three objectives.

1. Introduction

By fusing the respective advantages of manipulators with wheeled mobile bases, wheeled mobile manipulators (WMMs) are widely used in unstructured environments due to their dexterity, maneuverability, and mobility in complex scenarios. Besides, many tasks that require high accuracy are completed by deploying WMMs, including opening a door [1], rotating a valve [2], grabbing an object [3], and opening a drawer [4]. It is practical to extend the reach of a manipulator by adding a mobile base to it, as otherwise it would be limited to a settled workspace [5]. However, researchers usually establish the model of the WMM without considering the inherent differences between these two subsystems (mobile base and manipulator). For example, the base usually moves in an environment with complex dynamics (*e.g.*, slippage/skidding, or locomoting on uneven ground) while the manipulator is in free or contact motion [6]. Under such constraints, the existing high-precision operation methods for WMMs are mostly based on external perception information feedback. Studying how to improve WMMs' operation accuracy under circumstances without environmental information will reduce their dependence on external perception and broaden the adaptability of WMMs.

Due to the above-mentioned different characteristics of the mobile base and the manipulator, an unified modeling and motion planning framework of the entire system (called the mobile manipulator) should take these differences into

* This work was supported by Canada Foundation for Innovation (CFI), the Natural Sciences and Engineering Research Council (NSERC) of Canada, the Canadian Institutes of Health Research (CIHR), the Alberta Advanced Education Ministry, the Alberta Economic Development, Trade and Tourism Ministry's grant to Centre for Autonomous Systems in Strengthening Future Communities, the National Natural Science Foundation of China (Grant No. 51822502, U21B6002), State Key Laboratory of Robotics and Systems (HIT) (Grant No. SKLRS-2023-KF-04), the "111" Project (Grant No. B07018), and the China Scholarship Council under Grant [2019]06120165.

* Corresponding authors
** These authors contributed equally to this work.
xinghj@nuaa.edu.cn (H. Xing); gongzp@hit.edu.cn (Z. Gong); liangding@hit.edu.cn (L. Ding); ali.torabi@ualberta.ca (A. Torabi); chenjbao@nuaa.edu.cn (J. Chen); gaohaibo@hit.edu.cn (H. Gao); mahdi.tavakoli@ualberta.ca (M. Tavakoli)

account [7]. Fortunately, this combination often makes a WMM a kinematically redundant robotic system, which means it has more degrees of freedom (DOFs) than minimally required for performing tasks. While facing an infinite number of solutions, the WMM can provide a wealth of possibilities for the diversification of exercise options by selecting different joint motions, so as not to affect the posture (position and orientation) of the end-effector. Many different objectives have been achieved by using this inner joint motion, *e.g.*, manipulability enhancement, joint limitation avoidance, obstacle avoidance, and/or singularity avoidance [8, 9, 10, 11, 12].

Few studies, however, have addressed motion accuracy of a WMM's end-effector in absence of environment perception information, taking motion errors of the mobile base into account. As a result of discretizing a complex task, Shin *et al.* [13] enhanced the accuracy of the WMM by avoiding simultaneous activation of the mobile base and manipulator. Nagatani *et al.* [14] proposed a coordinated motion planning approach for a WMM to improve its kinematic precision. However, the inaccuracy of the mobile base's motion was neglected. Based on the assumption that the motion base had no motion inaccuracy, Papadopoulos *et al.* [15] proposed a motion planning approach for nonholonomic WMMs that simultaneously satisfied the nonholonomic constraints while maintaining the motions of the end-effector and the mobile base, respectively. Leoro and Hsiao [16] presented a method for planning the motions of nonholonomic mobile manipulators taking into account joint constraints and avoiding singularity/self-collisions. It was however ignored that the mobile base and manipulator had different motion accuracy, and the method cannot be used to solve hierarchical problems. Jia *et al.* [7] noticed the differences between the manipulator and the mobile base. For a nonholonomic mobile manipulator, the authors proposed an integrated motion planning approach using a weighted inverse Jacobian; however, the joint constraints (position, velocity, and acceleration) were not taken into account.

In our previous work [17], we used a weighting matrix to determine how the desired end-effector's motion of an omnidirectional WMM should be distributed to the movement of the mobile base and the behavior of the manipulator in order to improve the precision of the WMM's motion. A inverse Jacobian with a weighted component can be used to distribute motion between the mobile base and manipulator subsystems. However, if one joint exceeds its limit, the motion will simply be transferred from the manipulator to the mobile base, thus not fully exploiting the manipulator's redundancy [18].

This paper draws inspiration from the "saturation in the null space" (SNS) algorithm proposed by Flacco *et al.* [19, 20] for redundant manipulators and extends it to redundant mobile manipulators. Because of its ability to distribute end-effector motion to joint motion, the SNS method can address redundant systems' limitations effectively. However, it has never been utilized to improve the motion precision of a WMM. In view of this, we propose a novel adaptive multi-objective motion distribution framework (AMoMDiF) to improve WMMs' motion accuracy in circumstances without environment perception feedback. This framework adopts a hierarchical structure to explore the WMMs' null space iteratively for completing end-effector motion (primary objective), adaptive motion distribution (secondary objective), and singularity avoidance (tertiary objective). The motion accuracy enhancement is achieved by the secondary objective via distributing less of the end-effector motion to the mobile base. The tertiary goal is used to improve the capacity of the manipulator to stay away from a singular configuration.

The proposed framework includes an emphasis on examining the singularity of the manipulator first. It is possible to activate the mobile base at the same time if the manipulator is near a singular configuration. Due to this, the proposed method can only be performed when the manipulator is far enough away from a singularity. Additionally, the tertiary objective will be met without interfering with the primary and secondary objectives, in order to prevent a singularity from forming.

This paper is organized as follows. Section 2 presents the kinematics of a WMM. In Section 3, the proposed adaptive multi-objective motion distribution framework (AMoMDiF) is provided. The experimental results are reported in Section 4 to examine the performance of the proposed motion distribution framework. Concluding remarks appear in Section 5.

2. Kinematics of a Wheeled Mobile Manipulator

A typical wheeled mobile manipulator is usually composed of a wheeled mobile base and a manipulator. Thus, its kinematic model can be derived from the kinematic models of the two subsystems. A sketch of a WMM is shown in Fig. 1, where Σ_w, Σ_b, Σ_m, and Σ_{ee} represent the world reference frame, mobile base frame, manipulator reference frame, and end-effector frame, respectively.

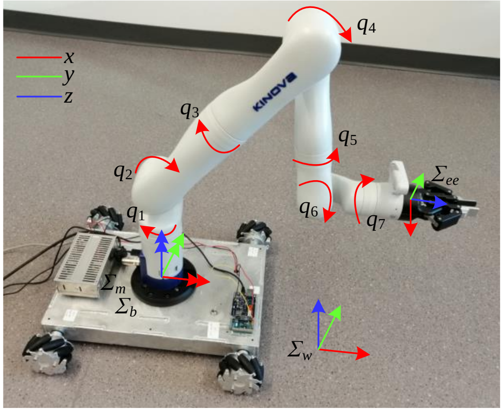

Figure 1: Sketch of a wheeled mobile manipulator.

First, assume that there is no slippage or skidding between the wheels of the mobile base and the ground (*i.e.*, pure rolling). Then we can express the mobile base's forward kinematics as $\dot{q}_b = \Psi(q_b)v_b$, where $q_b \in \mathbb{R}^{n_b}$ represents its generalized coordinate vector expressed in Σ_w, $v_b \in \mathbb{R}^b$ represents the wheels' velocity vector, $\Psi(q_b) \in \mathbb{R}^{n_b \times b}$ denotes its kinematic constraint matrix (holonomic or nonholonomic) that transfers the wheel velocities to the generalized mobile base velocities, and n_b and b represent the dimensions of the mobile base's generalized coordinate vector and the wheel velocity vector, respectively. Furthermore, both holonomic and nonholonomic mobile bases can apply to the above kinematic model.

The manipulator is usually subject to holonomic constraints, *i.e.*, its generalized velocity vector $\dot{q}_m \in \mathbb{R}^m$ can be assigned arbitrarily at any manipulator configurations, m denotes its dimension (number of joints). Here, we specify $v_m = \dot{q}_m$, where $v_m \in \mathbb{R}^m$ denotes the manipulator's joint input velocity vector.

The generalized coordinate vector and wheel/joint input velocity vector of the WMM are defined as $q = [q_b^{\mathrm{T}}, q_m^{\mathrm{T}}]^{\mathrm{T}} \in \mathbb{R}^n$ and $v = [v_b^{\mathrm{T}}, v_m^{\mathrm{T}}]^{\mathrm{T}} \in \mathbb{R}^{b+m}$, respectively, where $n = n_b + m$. Then, the forward kinematics at the velocity level for the entire WMM can be calculated as [21]

$$\dot{x} = J(q)\dot{q} = [J_b(q)\ J_m(q)] \begin{bmatrix} \dot{q}_b \\ \dot{q}_m \end{bmatrix} = [J_b(q)\Psi(q_b)\ J_m(q)] \begin{bmatrix} v_b \\ v_m \end{bmatrix} = J_v(q)v, \tag{1}$$

where $\dot{x} \in \mathbb{R}^r$ is the task-space velocity vector of the end-effector with its dimension being r, $J_b(q) \in \mathbb{R}^{r \times n_b}$ and $J_m(q) \in \mathbb{R}^{r \times m}$ denote the Jacobians of the mobile base and the manipulator, respectively. $J(q) \in \mathbb{R}^{r \times n}$ is the Jacobian of the unconstrained WMM (*i.e.*, no mobile base constraint is considered), and $J_v(q) \in \mathbb{R}^{r \times (b+m)}$ is the Jacobian of the WMM.

It should be mentioned that there are two Jacobians for WMMs due to the different locomotion of mobile bases, and this characteristic broadens the adaptability of our framework. In the presence of holonomic constraints on the mobile base, both $J(q)$ and $J_v(q)$ can be utilized. In the case of a nonholonomic mobile base, only $J_v(q)$ can be employed [22].

In most cases, a WMM system is kinematically redundant (*i.e.*, $r < n$). Thus, for an end-effector velocity $\dot{x}$, its inverse kinematics with null-space exploration considered can be expressed as[1]

$$\dot{q} = J^{\dagger}\dot{x} + (I - J^{\dagger}J)\dot{q}_{\mathcal{N}}, \tag{2}$$

where $J^{\dagger} = W^{-1}J^{\mathrm{T}}(JW^{-1}J^{\mathrm{T}})^{-1}$ denotes the weighted pseudoinverse of J with W being a symmetric and positive-definite weighting matrix, I represents an $n \times n$ identity matrix, $I - J^{\dagger}J$ is the $n \times n$ orthogonal projector in the Jacobian null space, and $\dot{q}_{\mathcal{N}} \in \mathbb{R}^n$ denotes a generic joint velocity. Eq. (2) presents the joint solution $\dot{q}$ that fulfills (1) (or minimizes $\|\dot{x} - J\dot{q}\|_2$ if the task cannot be completed), while minimizing in norm the distance to $\dot{q}_{\mathcal{N}}$.

In practical kinematic controller design, the inverse kinematics (2) can be expressed as[17, 23]

$$\dot{q} = J^{\dagger}\left[\dot{x}_d + K_x(x_d - x)\right] + (I - J^{\dagger}J)\dot{q}_{\mathcal{N}}, \tag{3}$$

[1] For brevity, the dependence of the Jacobian matrices upon the joint variables is omitted in the notation.

where $x \in \mathbb{R}^r$ and $x_d \in \mathbb{R}^r$ denote the actual and desired poses of the end-effector, respectively, and $K_x \in \mathbb{R}^{r\times r}$ is a diagonal positive-definite matrix. The end-effector velocity $\dot{x}$ in (2) is changed to $\dot{x}_d + K_x(x_d - x)$ in (3) to ensure that the motion tracking error converges to zero.

3. Adaptive Multi-objective Motion Distribution Framework

The mobile base of a WMM has less motion accuracy compared with the manipulator mounted on its top due to unknown ground-wheel contact, wheel wear or wheel slippage/skidding [7]. To improve the motion accuracy of the WMM in the absence of environment perception, an AMoMDiF is proposed. With this framework, the WMM can accomplish multiple objectives by exploring the WMM's null space iteratively in a hierarchical structure. In Section 3.1, the joint velocity limits are presented. Section 3.2 provides the basic motion distribution algorithm, taking the above joint limits into account. Section 3.3 discusses the singularity avoidance and mobile base motion issues. Finally, the structure of the proposed AMoMDiF is presented in Section 3.4.

3.1. Joint Velocity Limits Definition

This motion distribution approach is performed at the velocity level. Therefore, the limits on joint velocity need to be locally calculated considering the joint position, velocity, and acceleration bounds of the WMM. The velocity limits on $\dot{q}$ at the current WMM configuration q (time $t = t_h$) can be derived as

$$\dot{Q}_{\min}(q) \leqslant \dot{q} \leqslant \dot{Q}_{\max}(q) \tag{4}$$

with the velocity limits of each joint defined as [20]

$$\dot{Q}_{\min,i} = \max\left\{\frac{Q_{\min,i} - q_{i,h}}{T}, V_{\min,i}, -\sqrt{2A_{\max,i}(q_{i,h} - Q_{\min,i})}\right\}, \tag{5}$$

$$\dot{Q}_{\max,i} = \min\left\{\frac{Q_{\max,i} - q_{i,h}}{T}, V_{\max,i}, \sqrt{2A_{\min,i}(q_{i,h} - Q_{\max,i})}\right\}, \tag{6}$$

where $Q_{\max}/Q_{\min}$, $V_{\max}/V_{\min}$, and $A_{\max}/A_{\min}$ denote the maximum and minimum hard joint bounds of the position, velocity, and acceleration, respectively. $i = 1, \dots, n$ represents the i^{th} joint, T is the sampling time, and $q_{i,h}$ denotes the WMM's i^{th} joint position at current time t_h.

Here, we take (6) as an example to illustrate how to derive these velocity limits. The first term on its right-hand side is caused by the joint position constraint, the middle term is caused by its velocity constraints, and the third term is caused by its acceleration constraint. Thus, the largest joint velocity ought to be the minimum of the three. It is worth emphasizing that the third term is obtained by maximally decelerating the i^{th} joint when it approaches its upper position constraint.

3.2. Basic Motion Distribution Algorithm via Null-space Exploration

The proposed basic algorithm achieves the primary task (end-effector motion following) and the secondary objective (motion accuracy improvement) by exploring the WMM's null space iteratively. As the mobile base's motion precision is lower than that of the manipulator, it is desirable to distribute the end-effector motion requirement as much as possible to the manipulator to obtain high motion accuracy. Therefore, the mobile base will be activated only when the manipulator cannot complete the task.

In the proposed framework, a diagonal selection matrix S is employed to assign enabled joints. S is an $n\times n$ diagonal selection matrix whose diagonal elements are of one or zero specifying whether the joints are active or inactive, *i.e.*, if the j^{th} element on the S diagonal is one, the j^{th} joint is enabled. Then according to the selection matrix S and (2), the joint velocity command can be expressed as

$$\dot{q}_{amd} = (JS)^{\dagger}\varphi\dot{x} + [I - (JS)^{\dagger}J]\dot{q}_{\mathcal{N}}, \tag{7}$$

where φ represents a scaling factor used to curtail the end-effector motion requirement $\dot{x}$ when the WMM is not capable of meeting it. It is noteworthy that $\dot{q}_{amd}$ is a joint velocity solution when provided with end-effector velocity $\dot{x}$ and null-space velocity $\dot{q}_{\mathcal{N}}$. It will change to the usual pseudoinverse (minimum norm) solution $J^{\dagger}\dot{x}$ on the condition that $\varphi = 0$, $\mathcal{S} = I$, and $\dot{q}_{\mathcal{N}} = 0$. With this approach, there is no need for the complicated calculation mentioned in [24], which is performed at joint acceleration level.

At the outset, the selection matrix is selected as $\mathcal{S} = \begin{bmatrix} 0_{n_b \times n_b}, & 0 \\ 0, & I_{m\times m} \end{bmatrix}$; thus, no motion is distributed to the mobile base since it is disabled (the null-space velocity $\dot{q}_{\mathcal{N}}$ vector is chosen as a zero vector). Next, (7) is employed to calculate the joint velocity command. In detail, if the j^{th} joint of the manipulator is over-driven ($\dot{q}_{j,amd} > \dot{Q}_{\max,j}$ or $\dot{q}_{j,amd} < \dot{Q}_{\min,j}$), the corresponding element on the $\mathcal{S}$ diagonal is specified as zero to deactivate the joint, and the j^{th} element of $\dot{q}_{\mathcal{N}}$ is set equal to $\dot{Q}_{\max,j}$ or $\dot{Q}_{\min,j}$. The above operation on $\dot{q}_{\mathcal{N}}$ and $\mathcal{S}$ will set back the j^{th} joint velocity to its saturation level, and the corresponding velocity deficiency will be specified to other manipulator joints to conduct. This practice yet may overload the other joints of the manipulator. Thus, this approach needs to be reiterated until there is no over-driven joint remained. Otherwise, the end-effector velocity $\dot{x}$ is infeasible for the WMM with an immobilized mobile base.

The feasibility of the desired end-effector task $\dot{x}$ can be checked by the rank of $J\mathcal{S}$. In the case where the rank of this matrix is less than the dimension of the task-space motion r, then $\dot{x}$ is infeasible for the manipulator. Consequently, the mobile base should be enabled by changing the corresponding zeros in $\mathcal{S}$ to ones. When the mobile base is involved, all the WMM's joint velocities require to be recalculated according to (7). It is essential to downscale the required end-effector motion $\dot{x}$ to be partially accomplished if it cannot be completed by the WMM even with a mobile base that is enabled. To achieve this function, a scaling factor $0 \leqslant \varphi \leqslant 1$ is introduced for $\dot{x}$ to make it realizable. φ is equal to one unless $\dot{x}$ is infeasible for the WMM. Further description of φ will be detailed in 3.4.

3.3. Singularity Avoidance and Mobile Base Motion Issues

The above algorithm can make maximal use of the manipulator to perform the required end-effector motion. However, it sometimes propels the manipulator to the edge of its workspace and then launches the mobile base. During this process, workspace-boundary singularities are generated as the manipulator reaches its full extension. Thus, a revised version of the proposed framework should be presented to avoid singularity. We perform singularity avoidance in two levels. First, during each loop, if it is determined that the initial segment of the desired trajectory will make the manipulator approach one of its singularities, the mobile base is directly activated. Second, we add a tertiary objective to the WMM's null space to avoid paths that get close to them. We adopt the velocity manipulability ellipsoid, which is an effective measure to evaluate the distance of a robotic system from its singularity [25]. For a robotic manipulator, it is expressed as

$$\mathcal{H} = \sqrt{\det (J_m J_m^{\mathrm{T}})}. \tag{8}$$

A prioritized task motion plan ensures that the primary task is completed in a priority manner. It may also be possible to perform lower-priority tasks if there is still redundancy [26]. Here, the joint velocity command for the tertiary objective $\dot{q}_{\gamma}$ is devised as

$$\dot{q}_{\gamma} = \psi P_S \dot{q}_S, \tag{9}$$

where $0 \leqslant \psi \leqslant 1$ represents a scaling factor to respect the joint bounds when the remaining redundancy is not sufficient to hold it. In joint space, the subsidiary null-space projection matrix P_S is defined as follows,

$$P_S = \left[I - \left((I - \mathcal{S}) P_{\mathcal{N}} \right)^{\dagger} \right] P_{\mathcal{N}}, \tag{10}$$

where $P_{\mathcal{N}}$ denotes the Jacobian null space of the WMM with its definition being $P_{\mathcal{N}} = I - J^{\dagger} J$. The variable $\dot{q}_S$ denotes the joint velocity vector associated with the null-space projection matrix P_S, which is defined as

$$\dot{q}_S = k_N \begin{bmatrix} 0_{n_b \times 1} \\ (\nabla_{q_m} \mathcal{H})^{\mathrm{T}} \end{bmatrix} - k_D \dot{q}, \tag{11}$$

where k_N and k_D are positive constants. $k_D \dot{q}$ is a damping term to stabilize the system. The joint velocity command that achieves the desired end-effector motion, follows the motion distribution method, and fits the tertiary objective can be expressed as

$$\dot{q} = \dot{q}_{amd} + \dot{q}_{\gamma}. \tag{12}$$

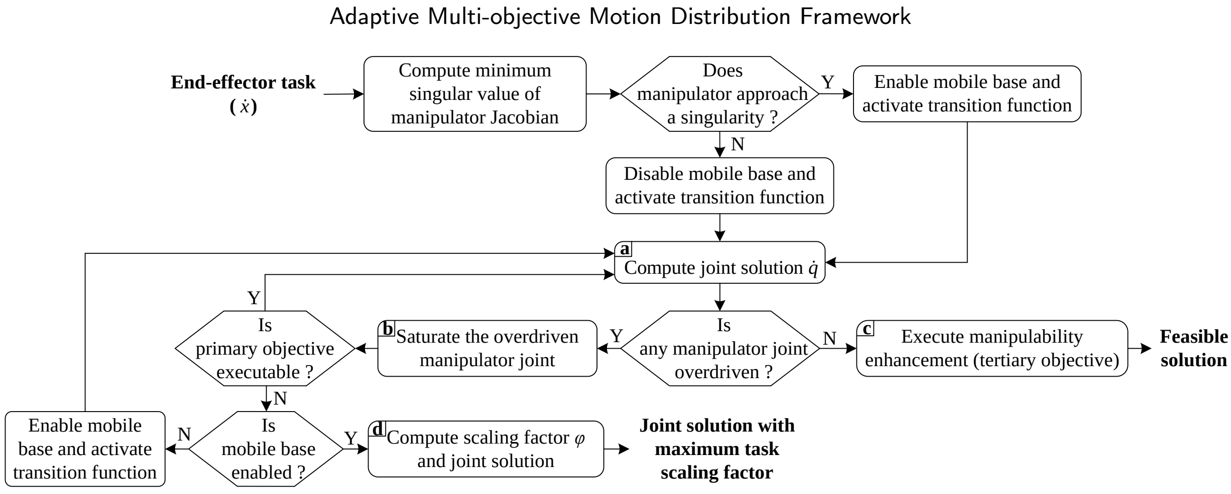

Figure 2: Flowchart of the proposed AMoMDiF for a WMM.

We note that the proposed framework is realized at the joint velocity level. Thus, once the mobile base is suddenly enabled or disabled, the instant velocity command may vibrate the WMM. This phenomenon ought to be avoided to improve the WMM's motion accuracy. Therefore, a transition function is adopted to launch/stop the mobile base stably

$$\dot{q}_{b,tr} = \begin{cases} 0 \,/\, \dot{q}_b, & \text{if } t \leqslant t_s \\ V_b \frac{t-t_s}{t_f^+ - t_s} \,/\, V_b \frac{t_f^+ - t}{t_f^+ - t_s}, & \text{if } \begin{cases} \text{sign}(V_b) > 0 \\ t_s < t < t_f^+ \end{cases} \\ V_b \frac{t-t_s}{t_f^- - t_s} \,/\, V_b \frac{t_f^- - t}{t_f^- - t_s}, & \text{if } \begin{cases} \text{sign}(V_b) < 0 \\ t_s < t < t_f^- \end{cases} \\ \dot{q}_b \,/\, 0, & \text{if } \begin{cases} \text{sign}(V_b) > 0 \\ t \geqslant t_f^+ \end{cases} \\ \dot{q}_b \,/\, 0, & \text{if } \begin{cases} \text{sign}(V_b) < 0 \\ t \geqslant t_f^- \end{cases} \end{cases} \tag{13}$$

where $\dot{q}_{b,tr}$ denotes the mobile base velocity during the transition procedure, t_s and $t_f^+(t_f^-)$ denote the start and final time of the transition, respectively. In (13), the first value denotes the start condition, and the second value represents the stop condition. V_b represents the base velocity when it starts to activate/deactivate. $t_f^+ = |\frac{V_b}{A_{\min,b}}| + t_s$ and $t_f^- = |\frac{V_b}{A_{\max,b}}| + t_s$, where $A_{\max,b}$ and $A_{\min,b}$ denote the maximum and minimum accelerations of the base, respectively.

3.4. Illustration of the Adaptive Multi-objective Motion Distribution Framework

The complete procedure of the proposed AMoMDiF is presented in Fig. 2 and **Algorithm** 1, and an approach to regulate the scaling factors φ (in (7)) and ψ (in (9)) is shown in **Algorithm** 2.

Fig. 2 and **Algorithm** 1 show the proposed framework to realize motion distribution for a WMM, taking singularity avoidance into account. The primary task is to achieve the desired end-effector's motion, and the secondary mission is to distribute the end-effector motion requirement as much as possible to the manipulator. In this study, the mobile base is deactivated until the manipulator approaches a singularity or saturated.

The minimum singular value of the manipulator Jacobian matrix J_m [27] is employed to detect the manipulator's singularity, which is denoted as σ_m and the singularity measure here is specified as $\sigma_{m,min}$. It is noteworthy that the maximization of $\mathcal{H}$ in (8) can enlarge σ_m. Suppose $\sigma_m < \sigma_{m,min}$, indicating that the manipulator is close to a singularity. Then, the mobile base will be activated to move the manipulator away from it by kinematic reconfiguration. Further, when the WMM has remaining redundancy after the primary and secondary tasks are realized, the tertiary objective

Algorithm 1 Adaptive motion distribution algorithm.

Initialization: $\mathcal{S} = \begin{bmatrix} 0_{n_b \times n_b}, & 0 \\ 0, & I_{m\times m} \end{bmatrix}$, $\sigma_{m,min}$, r

Steps:

Compute σ_m
if $\sigma_m < \sigma_{m,min}$ **then**
  $\mathcal{S}_{n_b\times n_b} = I_{n_b\times n_b}$ and activate (13)
else
  $\mathcal{S}_{n_b\times n_b} = 0_{n_b\times n_b}$ and activate (13)
end if
$\dot{q}_{amd} = (J\mathcal{S})^{\dagger}\dot{x} + [I - (J\mathcal{S})^{\dagger}J]\dot{q}_{\mathcal{N}}$ } **a**
if $\exists j \in [1:m] : \dot{q}_{j,amd} > \dot{Q}_{\max,j} || \dot{q}_{j,amd} < \dot{Q}_{\min,j}$ **then**
  repeat
    k={most critical joint}
    $\mathcal{S}_{kk} = 0$
    $\dot{q}_{\mathcal{N},k} = \begin{cases} \dot{Q}_{\max,k}, & \text{if } \dot{q}_{k,amd} > \dot{Q}_{\max,k} \\ \dot{Q}_{\min,k}, & \text{if } \dot{q}_{k,amd} < \dot{Q}_{\min,k} \end{cases}$ } **b**
    if rank($J\mathcal{S} \geqslant r$) **then**
      $\dot{q}_{amd} = (J\mathcal{S})^{\dagger}\dot{x} + [I - (J\mathcal{S})^{\dagger}J]\dot{q}_{\mathcal{N}}$
    else
      if $\mathcal{S}_{n_b\times n_b} = I_{n_b\times n_b}$ **then**
        Compute scaling factor φ
        $\dot{q}_{amd} = (J\mathcal{S})^{\dagger}\varphi\dot{x} + [I - (J\mathcal{S})^{\dagger}J]\dot{q}_{\mathcal{N}}$ } **d**
        go to `marker`
      else
        $\mathcal{S}_{n_b\times n_b} = I_{n_b\times n_b}$ and activate (13)
        $\dot{q}_{amd} = (J\mathcal{S})^{\dagger}\dot{x} + [I - (J\mathcal{S})^{\dagger}J]\dot{q}_{\mathcal{N}}$
      end if
    end if
  until $\forall j \in [1:m] : \dot{Q}_{\min,j} \leqslant \dot{q}_{j,amd} \leqslant \dot{Q}_{\max,j}$
else
  Activate (9)–(11)
  Compute scaling factor ψ and $\dot{q}_{\gamma}$ } **c**
end if
`marker:`
Calculate joint velocity command with (12)

with (9)–(11) will be conducted to enhance the manipulator's ability to stay away from a singularity. If the primary task or the tertiary task cannot be fully realized, a scaling factor φ or ψ is utilized to make it partially executed.

Algorithm 2 presents the procedure of regulating the two scaling factors according to the joint bounds (4)-(6). The variable λ represents the needed joint velocity for the previous task, and ξ denotes the consuming joint motion capability of the manipulator for the primary or the tertiary task. Then, the ratio of the residual joint velocity to the required joint velocity (denoting as $\rho_{\min}$ and $\rho_{\max}$) is calculated, and the minimum ratio of all the joints is obtained, expressed as Φ. The variable Φ is a criterion showing the residual capacity of the manipulator to complete the task. Suppose $\Phi \geqslant 1$, the manipulator has sufficient capacity to achieve the task. $\Phi < 1$ indicates the manipulator cannot accomplish the task. The desired end-effector task should not be upscaled; thus, the scaling factor (φ or ψ) is selected as the smaller between Φ and 1.

4. Experimental Results

To verify the effectiveness of the proposed AMoMDiF, it was implemented on a wheeled mobile manipulator. A traditional motion planning approach that employed the pseudoinverse of the WMM's Jacobian was implemented as a control group (to be fair, we extended it to perform manipulability enhancement). Alternatively, you may choose

Algorithm 2 Scaling factor regulation.

Initialization: φ: $\left\{ \begin{array}{c} \lambda = (JS)^{\dagger}\dot{x} \\ \xi = [I - (JS)^{\dagger}J]\dot{q}_{\mathcal{N}} \end{array} \right\}$; ψ: $\left\{ \begin{array}{c} \lambda = P_S \dot{q}_S \\ \xi = \dot{q}_{amd} \end{array} \right\}$

Steps:

$\rho_{\min} = (\dot{Q}_{\min} - \xi)/\lambda$, $\rho_{\max} = (\dot{Q}_{\max} - \xi)/\lambda$
for $i = 1 \rightarrow m$ **do**
  if $\rho_{\min,i} > \rho_{\min,i}$ **then**
    Switch $\rho_{\min,i}$ and $\rho_{\max,i}$
  end if
  $\Phi = \min\{\rho_{\max,i}\}$
end for
Scaling factor (φ or ψ) = $\min\{\Phi, 1\}$

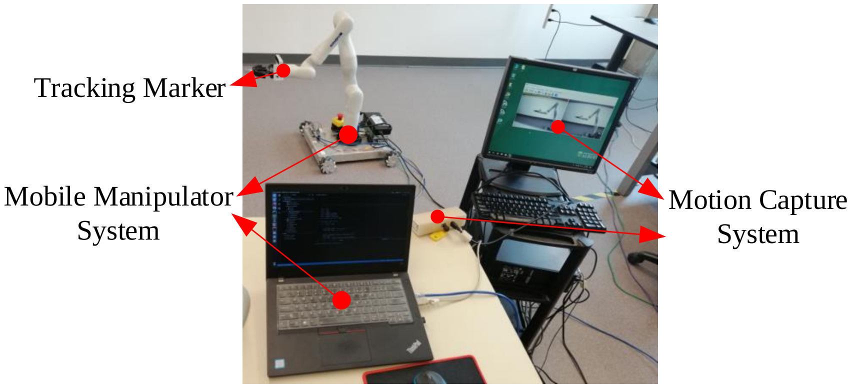

Figure 3: Experimental setup. Mobile manipulator system consists of an omnidirectional WMM and a computer; motion capture system is composed of a binocular camera and a computer; tracking marker is a target to be tracked by the motion capture system. The subsystems are connected via the UDP/IP Ethernet protocol.

the quadratic programming (QP) method [28] as the traditional motion planning approach, but it has some limitations, including the high computational load that results from the increase in DOFs and the possibility of multiple hierarchical tasks or impractical tasks. In comparison to pseudoinverse-based techniques, it is less suitable.

The experiments comprise two units: (A) the confirmation of the necessity of singularity avoidance and (B) evaluating the proposed motion distribution framework.

4.1. Experimental Setup

The experiments were conducted with an omnidirectional WMM, which is composed of a custom-built four-wheel mobile base and a 7-DOF ultra-lightweight robotic arm Kinova Gen3 (Kinova Robotics, Canada), as shown in Fig. 1. As a result of the mobile base's four Mecanum wheels, omnidirectional movement is possible. The motion planning code was developed in C++, adopting the Eigen library [29] for algebraic computations. The experiments were performed in the ROS environment [30] on a Intel(R) Xeon(R) CPU X5550 @ 2.67 GHz, with 16 GB of RAM.

Fig. 3 presents the setup for the experiment, which consists of a self-assembled WMM and a motion capture system (Claron Technology Inc., Canada). The RMS value of the motion capture system's calibration precision is 0.35 mm. It deserves attention that the motion capture system is utilized solely for determining the end-effector's actual position to evaluate the motion accuracy of the proposed framework and not used for motion planning.

The WMM we employed in our experiment is an omnidirectional one and we chose J as its Jacobian, as defined in (1). The mobile base's kinematics representation is shown in Fig. 4, where its generalized coordinate vector is denoted as $q_b = [x_b, y_b, \theta_b]^{\mathrm{T}} \in \mathbb{R}^3$ and the wheels' velocity command vector as $v_b = [\omega_1, \omega_2, \omega_3, \omega_4]^{\mathrm{T}} \in \mathbb{R}^4$. The matrix $\Psi(q_b) \in \mathbb{R}^{3\times4}$, which is employed to transfer the wheel velocity to the generalized base velocity, can be derived as

$$\Psi(q_b) = J_\alpha J_\beta, \tag{14}$$

Table 1
Joint constraints of the WMM. Joints corresponding to the mobile base are the first three; joints corresponding to the manipulator are the rest seven.

Joint No.	Angle	Velocity	Acceleration
1	$\pm\infty$	± 0.25 m/s	± 0.025 m/s^2
2	$\pm\infty$	± 0.25 m/s	± 0.025 m/s^2
3	$\pm\infty$	± 1.0 rad/s	± 1.5 rad/s^2
4	$\pm\infty$	± 1.75 rad/s	± 3.0 rad/s^2
5	± 2.2 rad	± 1.75 rad/s	± 3.0 rad/s^2
6	$\pm\infty$	± 1.75 rad/s	± 3.0 rad/s^2
7	± 2.5 rad	± 1.75 rad/s	± 3.0 rad/s^2
8	$\pm\infty$	± 3.14 rad/s	± 5.0 rad/s^2
9	± 2 rad	± 3.14 rad/s	± 5.0 rad/s^2
10	$\pm\infty$	± 3.14 rad/s	± 5.0 rad/s^2

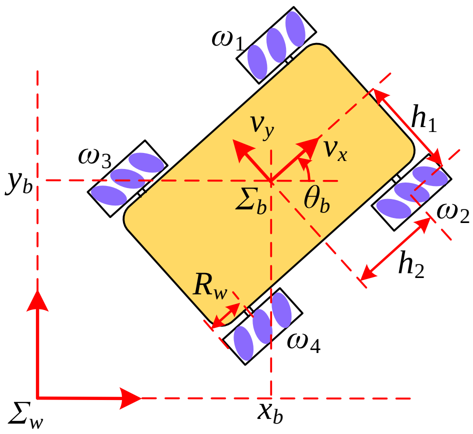

Figure 4: Kinematics of the omnidirectional mobile base.

with

$$J_\alpha = \begin{bmatrix} \cos\theta_b & -\sin\theta_b & 0 \\ \sin\theta_b & \cos\theta_b & 0 \\ 0 & 0 & 1 \end{bmatrix},$$

and

$$J_\beta = \frac{R_w}{4} \begin{bmatrix} 1 & 1 & 1 & 1 \\ -1 & 1 & 1 & -1 \\ \frac{-1}{h_1+h_2} & \frac{1}{h_1+h_2} & \frac{-1}{h_1+h_2} & \frac{1}{h_1+h_2} \end{bmatrix}.$$

The meaning of the variables θ_b, R_w, h_1, and h_2 are illustrated in Fig. 4.

Table 1 shows the joint constraints of the WMM, where the first two joints are prismatic joints and the remaining eight are revolute joints. We note that the joint configuration of the mobile base is selected as its generalized coordinate vector since its wheel motions are not entirely independent. The task-space dimension of the WMM's end-effector is defined as $r = 3$, considering the end-effector's position. The mobile base frame Σ_b is presumed to be overlapped with the world reference frame Σ_w at the beginning of the experiment.

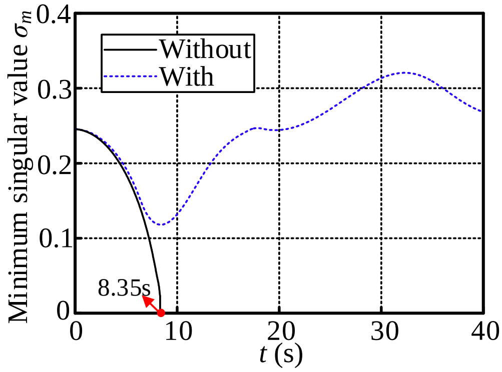

(a) σ_m

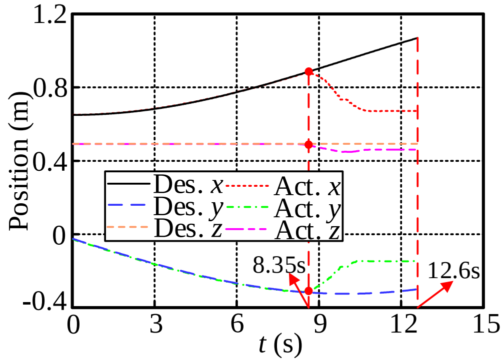

(b) End-effector position

Figure 5: Results of singularity avoidance experiment. The left figure provides the minimum singular value σ_m of the manipulator's Jacobian, and the right figure presents the end-effector position with the proposed framework but without singularity avoidance.

4.2. Experimental Demonstration of Singularity Avoidance

If no singularity avoidance is implemented, the AMoMDiF can sometimes bring the manipulator to a singularity. Thus, the consideration of singularity avoidance is inevitable, albeit it will somewhat decrease the WMM's motion accuracy as the mobile base is activated. There is actually a trade-off between the WMM's motion accuracy and the manipulator's singularity, depending on whether the mobile base is enabled or not. Earlier deployment of a mobile base will cause the manipulator to be farther away from the singularity, and WMM's motion accuracy will be lower.

The AMoMDiF and the modified AMoMDiF (*i.e.*, the AMoMDiF with singularity avoidance) were experimentally compared to verify the advantages of the latter. During the experiment, the desired end-effector trajectory is defined as a circle with a radius of 0.25 m. It is worth mentioning that this radius surpasses the manipulator workspace, which is 0.2 m with its initial configuration. The motion planning parameters are set as $K_x = 10I_{3\times3}$, $k_N = 5$, $k_D = 0.5$, and $\sigma_{m,min} = 0.15$. These parameters are provided because they are necessary to fulfill the motion planner design, but they do not occupy a critical position in enhancing the WMM's motion precision. Fig. 5 presents the results of the singularity avoidance experiment.

Fig. 5a shows the results with and without singularity avoidance. The minimum singular value σ_m of the WMM's Jacobian is adopted as the singularity index. In the absence of singularity avoidance, the manipulator strove to accomplish the task on its own and finally reached a singular configuration at approximately 8.35 s. This result made the system uncontrollable and prevented the task from being completed. However, if the proposed singularity avoidance method was employed (singularity supervision and manipulability enhancement), the mobile base was activated, and the manipulator adjusted its configuration to move away from a singularity when the manipulator approached it. As a result, it is still possible to accomplish the task. Fig. 5b shows the position of the end-effector when no singularity avoidance was used. In that case, the desired trajectory was unable to be followed at about 8.35 s, and substantial motion errors began to occur in all directions. This section does not include the position result with singularity avoidance since it will be discussed in more detail afterwards.

4.3. Experiments for Motion Accuracy Improvement

It is possible to take full advantage of the manipulator to perform tasks while keeping it from a singularity with the presented kinematic motion distribution framework. The mobile base is activated only when the manipulator cannot complete the assignment or when the manipulator reaches a singular configuration. Thus, the mobile base motion under the desired WMM's end-effector motion is minimized, enhancing the motion accuracy of the WMM.

A predefined end-effector trajectory was used to evaluate the efficiency of the proposed motion distribution framework in comparison with a traditional kinematic motion planner. The employment of the pseudoinverse of the Jacobian $J^{\dagger} = J^{\mathrm{T}}(JJ^{\mathrm{T}})^{-1}$ with manipulability enhancement for the manipulator in its null space [31] is considered as the traditional motion planner. Two desired trajectories are provided. The first one is within the manipulator workspace, a circle with a radius of 0.1 m. The second one is beyond the manipulator workspace, a circle with a radius of 0.25 m. The motion planning parameters in the experiments are the same as those in the first experiment, and the results of these

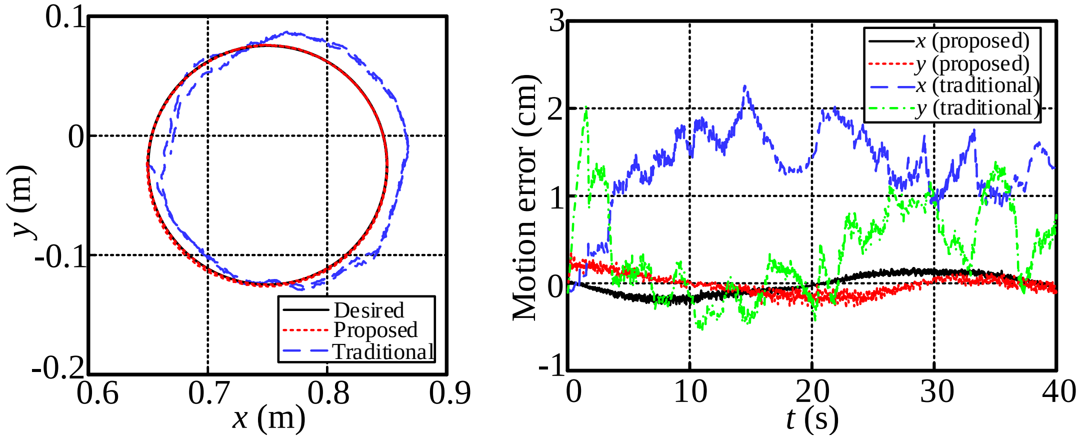

(a) End-effector trajectories (b) Motion errors

Figure 6: End-effector's motion accuracy with traditional and proposed methods (within manipulator workspace).

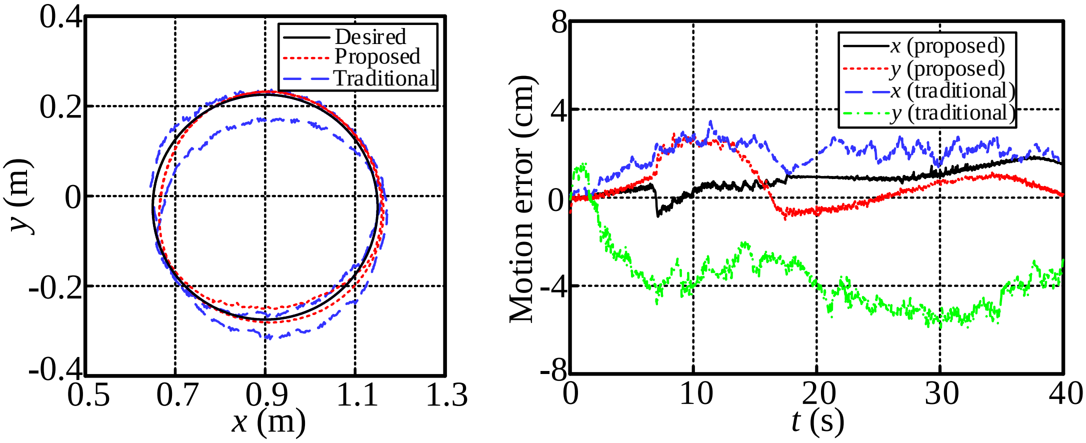

(a) End-effector trajectories (b) Motion errors

Figure 7: End-effector's motion accuracy with traditional and proposed methods (beyond manipulator workspace).

two experiments are shown in Fig. 6 and Fig. 7, respectively. The motion capture system was used to obtain ground-truth information about the actual position of the end-effector. The RMS value and duration time of the commanded mobile base velocity in these two conditions are provided in Table 2.

Fig. 6a shows that with the proposed framework, there was only a tiny motion error when the desired end-effector trajectory was within the manipulator workspace. This desirable experimental result is induced by the fact that no motion was specified to the mobile base, as shown in the first column of Table 2. With no adaptive motion distribution, some motions were assigned to the mobile base, as shown in the second column of Table 2. In this case, the motion error was much more significant compared with the motion distribution scenario because of the low motion accuracy of the mobile base (as illustrated in Fig. 6b). A maximum error of 2.26 cm was observed on the x-axis and 2.04 cm was observed on the y-axis.

When the desired end-effector motion was beyond the manipulator workspace, indicating the manipulator could not complete the task alone, then the mobile base was always forced to be actuated, as shown in the last two columns of Table 2. It must be noted, however, that the movement of the mobile base was much smaller if the proposed AMoMDiF was used. The commanded duration and RMS value of the mobile base velocity in x_b, y_b, and θ_b only took up 26.95%, 56.67%, 35.75%, and 36.65% of the commands without motion distribution, respectively. The end-effector motion

Table 2
Motion of the mobile base.

		Within workspace		Beyond workspace	
		Proposed	Traditional	Proposed	Traditional
x_b	RMS (cm/s)	0	1.09	1.53	2.7
	Duration (s)	0	40	10.78	40
y_b	RMS (cm/s)	0	0.59	0.54	1.51
	Duration (s)	0	40	10.78	40
θ_b	RMS (°/s)	0	0.229	0.206	0.562
	Duration (s)	0	40	10.78	40

accuracy results are presented in Fig. 7. Fig. 7b shows that the maximum motion errors in x and y were reduced from 3.47 cm to 1.81 cm, and from 5.93 cm to 2.62 cm contrasted with no motion distribution condition, respectively.

In this paper, the motion accuracy of a WMM can be improved with our proposed framework. However, we only consider the kinematic motion here; thus, some challenges still exist to enhance the WMM's dynamic motion accuracy. In the future, we will investigate both the dynamic and kinematic accuracy of the system.

5. Conclusions

This paper presented an adaptive multi-objective motion distribution framework (AMoMDiF) to improve the motion accuracy of a wheeled mobile manipulator (WMM) in the absence of environment perception feedback. The presented framework tried its best to transfer more motions to the manipulator to enhance the WMM's motion accuracy due to the lower kinematic accuracy of the wheeled locomotion. Its significant performance lies in that the mobile base was immobile until all the redundancy of the manipulator for the task was depleted, or the manipulator was close to a singularity. If the remaining unsaturated joints of the manipulator were not sufficient to execute the task, then the motion planner would distribute some motions to the mobile base. Also, we utilized the task priority method to designate manipulability enhancement as a tertiary task to avoid singularities. To sum up, when the primary task (end-effector motion achievement) and the secondary task (adaptive motion distribution) were resolved, the remaining DOFs were able to be used to keep the manipulator away from the singularity (tertiary task).

Several experiments were performed to compare the proposed method with a traditional approach by achieving several given end-effector trajectories. When the predefined end-effector trajectory surpassed the manipulator workspace, the maximum motion errors of the end-effector in x axis and y axis were enhanced by 47.8% and 55.8%, respectively, and the motion duration of the mobile base was reduced by 73.1%. Our future work will focus on creating the WMM's dynamic model and enhancing both its kinematic and dynamic motion precision.

References

[1] H. Xing, L. Ding, H. Gao, W. Li, M. Tavakoli, Dual-user haptic teleoperation of complementary motions of a redundant wheeled mobile manipulator considering task priority, IEEE Transactions on Systems, Man, and Cybernetics: Systems 52 (10) (2022) 6283–6295.

[2] S. R. Ahmadzadeh, P. Kormushev, R. S. Jamisola, D. G. Caldwell, Learning reactive robot behavior for autonomous valve turning, in: IEEE/RAS International Conference on Humanoid Robots, 2014, pp. 366–373.

[3] P. Štibinger, G. Broughton, F. Majer, Z. Rozsypálek, A. Wang, K. Jindal, A. Zhou, D. Thakur, G. Loianno, T. Krajník, M. Saska, Mobile manipulator for autonomous localization, grasping and precise placement of construction material in a semi-structured environment, IEEE Robotics and Automation Letters 6 (2) (2021) 2595–2602.

[4] T. Yamamoto, K. Terada, A. Ochiai, F. Saito, Y. Asahara, K. Murase, Development of the research platform of a domestic mobile manipulator utilized for international competition and field test, in: IEEE/RSJ International Conference on Intelligent Robots and Systems, 2018, pp. 7675–7682.

[5] J. Chen, P. I. Ro, Human intention-oriented variable admittance control with power envelope regulation in physical human-robot interaction, Mechatronics 84 (2022) 102802.

[6] W. Li, L. Ding, H. Gao, M. Tavakoli, Haptic tele-driving of wheeled mobile robots under nonideal wheel rolling, kinematic control and communication time delay, IEEE Transactions on Systems, Man, and Cybernetics: Systems 50 (1) (2020) 336–347.

[7] Y. Jia, N. Xi, Y. Cheng, S. Liang, Coordinated motion control of a nonholonomic mobile manipulator for accurate motion tracking, in: IEEE/RSJ International Conference on Intelligent Robots and Systems, 2014, pp. 1635–1640.

[8] J. Woolfrey, W. Lu, D. Liu, A control method for joint torque minimization of redundant manipulators handling large external forces, Journal of Intelligent & Robotic Systems 96 (1) (2019) 3–16.

[9] B. Bayle, J.-Y. Fourquet, M. Renaud, Manipulability of wheeled mobile manipulators: Application to motion generation, The International Journal of Robotics Research 22 (7-8) (2003) 565–581.

[10] H. Zhang, Y. Jia, N. Xi, Sensor-based redundancy resolution for a nonholonomic mobile manipulator, in: IEEE/RSJ International Conference on Intelligent Robots and Systems, 2012, pp. 5327–5332.

[11] J. Li, H. Gao, Y. Wan, J. Humphreys, C. Peers, H. Yu, C. Zhou, Whole-body control for a torque-controlled legged mobile manipulator, Actuators 11 (11) (2022) 304.

[12] A. Torabi, M. Khadem, K. Zareinia, G. R. Sutherland, M. Tavakoli, Application of a redundant haptic interface in enhancing soft-tissue stiffness discrimination, IEEE Robotics and Automation Letters 4 (2) (2019) 1037–1044.

[13] D. H. Shin, B. S. Hamner, S. Singh, M. Hwangbo, Motion planning for a mobile manipulator with imprecise locomotion, in: IEEE/RSJ International Conference on Intelligent Robots and Systems, 2003, pp. 847–853.

[14] K. Nagatani, T. Hirayama, A. Gofuku, Y. Tanaka, Motion planning for mobile manipulator with keeping manipulability, in: IEEE/RSJ International Conference on Intelligent Robots and Systems, 2002, pp. 1663–1668.

[15] E. Papadopoulos, J. Poulakakis, Planning and model-based control for mobile manipulators, in: IEEE/RSJ International Conference on Intelligent Robots and Systems, 2000, pp. 1810–1815.

[16] J. Leoro, T. Hsiao, Motion planning of nonholonomic mobile manipulators with manipulability maximization considering joints physical constraints and self-collision avoidance, Applied Sciences 11 (14) (2021) 6509.

[17] H. Xing, A. Torabi, L. Ding, H. Gao, Z. Deng, M. Tavakoli, Enhancement of force exertion capability of a mobile manipulator by kinematic reconfiguration, IEEE Robotics and Automation Letters 5 (4) (2020) 5842–5849.

[18] G. Antonelli, S. Chiaverini, Fuzzy redundancy resolution and motion coordination for underwater vehicle-manipulator systems, IEEE Transactions on Fuzzy Systems 11 (1) (2003) 109–120.

[19] F. Flacco, A. De Luca, O. Khatib, Motion control of redundant robots under joint constraints: Saturation in the null space, in: IEEE International Conference on Robotics and Automation, 2012, pp. 285–292.

[20] F. Flacco, A. De Luca, O. Khatib, Control of redundant robots under hard joint constraints: Saturation in the null space, IEEE Transactions on Robotics 31 (3) (2015) 637–654.

[21] A. De Luca, G. Oriolo, P. R. Giordano, Kinematic modeling and redundancy resolution for nonholonomic mobile manipulators, in: IEEE International Conference on Robotics and Automation, 2006, pp. 1867–1873.

[22] H. Xing, A. Torabi, L. Ding, H. Gao, Z. Deng, V. K. Mushahwar, M. Tavakoli, An admittance-controlled wheeled mobile manipulator for mobility assistance: Human–robot interaction estimation and redundancy resolution for enhanced force exertion ability, Mechatronics 74 (2021) 102497.

[23] V. Rayankula, P. M. Pathak, Fault tolerant control and reconfiguration of mobile manipulator, Journal of Intelligent & Robotic Systems 101 (2) (2021) 1–18.

[24] H. Xing, A. Torabi, L. Ding, H. Gao, W. Li, M. Tavakoli, Enhancing kinematic accuracy of redundant wheeled mobile manipulators via adaptive motion planning, Mechatronics 79 (2021) 102639.

[25] T. Yoshikawa, Manipulability of robotic mechanisms, The International Journal of Robotics Research 4 (2) (1985) 3–9.

[26] F. Flacco, A. De Luca, O. Khatib, Prioritized multi-task motion control of redundant robots under hard joint constraints, in: IEEE/RSJ International Conference on Intelligent Robots and Systems, 2012, pp. 3970–3977.

[27] S. Chiaverini, Singularity-robust task-priority redundancy resolution for real-time kinematic control of robot manipulators, IEEE Transactions on Robotics and Automation 13 (3) (1997) 398–410.

[28] M. Giftthaler, F. Farshidian, T. Sandy, L. Stadelmann, J. Buchli, Efficient kinematic planning for mobile manipulators with non-holonomic constraints using optimal control, in: IEEE International Conference on Robotics and Automation, 2017, pp. 3411–3417.

[29] G. Guennebaud, B. Jacob, et al., Eigen v3, URL: http://eigen. tuxfamily. org (2010).

[30] M. Quigley, K. Conley, B. Gerkey, J. Faust, T. Foote, J. Leibs, R. Wheeler, A. Y. Ng, ROS: An open-source robot operating system, in: ICRA workshop on open source software, Kobe, Japan, 2009.

[31] F. Vigoriti, F. Ruggiero, V. Lippiello, L. Villani, Control of redundant robot arms with null-space compliance and singularity-free orientation representation, Robotics and Autonomous Systems 100 (2018) 186–193.